Spectrochimica Acta Part B: Atomic Spectroscopy 243 (2026) 107586

Contents lists available at ScienceDirect

Spectrochimica Acta Part B: Atomic Spectroscopy

journal homepage: www.elsevier.com/locate/sab

Film-like residue preparation by drop on demand picoliter printing for TXRF analysis☆

Franziska Sand [a,*], Sven Hampel [a,b], Giancarlo Pepponi [c], Ursula Elisabeth Adriane Fittschen [a]

[a] Clausthal University of Technology, Institute of Inorganic and Analytical Chemistry, Arnold-Sommerfeld Straße 4, Clausthal-Zellerfeld, 38678, Germany
[b] Deutsches Elektronen Synchrotron DESY, Notkestraße 85, Hamburg, 22607, Germany
[c] Fundazione Bruno Kessler, Sensors and Devices, Micro Nano Facility, via Sommarive 18, Trento, 38123, Italy

ARTICLE INFO

Keywords:
Thermal inkjet printing
Picoliter printing
Film-like residue morphology
TXRF
GIXRF
AFM
Static elimination

ABSTRACT

An accurate sample preparation is substantial for obtaining reliable results in total reflection X-ray fluorescence analysis (TXRF). Pipetting of sample solutions in the microliter range often leads to "coffee rings" where the specimen dries inhomogeneously with a mixed morphology (film-like in the center and particle-like at the ring). The specimen morphology can be controlled in a more reliable manner by picoliter printing achieving particle-like residues.

The preparation of film-like residues is in general more challenging. It requires the optimization of the printing procedure, *e.g.* the deposited mass, additives as well as the elimination of static charges. Influences of different additives on the film formation were experimentally probed. The aim of this study was to develop a reliable method to improve the film formation of nickel on quartz reflectors, which are commonly used as sample carriers in TXRF. Nickel was chosen because it has a good sensitivity in TXRF and is often used as reference when studying the TXRF instrument performance. Grazing incidence X-ray fluorescence analysis (GIXRF) was used evaluating the morphology of the residues. The use of additives and variation of printing parameters improved the film formation slightly. The elimination of static charges was the most critical parameter in order to achieve films. The combination of Triton X-100 as a non-ionic surfactant with the static elimination yielded near-perfect films (≈1 ng Ni). The film morphology was investigated by atomic force microscopy, however the results were inconclusive.

1. Introduction

Ultra-trace analysis techniques like total reflection X-ray fluorescence analysis (TXRF) require an accurate sample preparation [1,2]. Depending on the analyte type and its physical state, the pretreatment strategies vary from minimal or no sample treatment to mineralization or extraction procedures [1]. In most cases an aqueous solution is applied to reflectors commonly made out of quartz glass, acrylic, boron nitride or glassy carbon and dried to residues [2]. The quartz glass carriers (30 mm in diameter and 3 mm in height) are commonly siliconized before the sample preparation process to obtain a hydrophobic surface [1]. The liquid sample is then applied onto the sample carrier using a micropipette and dried on a heating plate or under infrared light [1]. Ideally, a homogeneous residue is obtained, while often so-called "coffee rings" result from capillary flow [2,3]. During the drying process, the contact line between liquid and reflector is pinned and drying of the solution causes an outward flow within the droplet [3]. Thus, the sample dries inhomogeneously where the outer part of the dried deposit accumulates more mass than the inner part [4]. The transport properties of the dissolved ions may also differ in the convective flow. If the analyte and internal standard (IS) dry inhomogeneously on the carrier, the assumption of an ideal elemental distribution is no longer valid and quantification is biased resulting in over- or underestimation [4]. Further "coffee ring" structures or distorted residues are obtained by scratches on the sample carriers as they are able to pin the contact line of the droplet during the drying process [3,5,6].

By applying smaller volumes on the reflector in the nanoliter or picoliter range the particular character of the residues is improved and an inhomogeneous elemental distribution due to extended "coffee rings" can be minimized [2,7]. Picoliter printing for X-ray fluorescence analysis is quite new and was first used by Fittschen et al. for

☆ This article is part of a Special issue entitled: 'TXRF2025' published in Spectrochimica Acta Part B: Atomic Spectroscopy.

* Corresponding author.
E-mail address: franziska.sand@tu-clausthal.de (F. Sand).

https://doi.org/10.1016/j.sab.2026.107586
Received 27 March 2026; Received in revised form 9 June 2026; Accepted 10 June 2026
Available online 16 June 2026

deposition of standards in aerosol analysis with TXRF [8]. Further studies showed that picoliter droplets implemented as a reliable tool to be used in a broad application field as a reference in micro X-ray fluorescence (mXRF) [9], in semiconductor applications [6] and for the determination of the detector field of view in a laboratory TXRF spectrometer [4].

Inkjet techniques are commonly established in offices, or for printing newspapers, but are also frequently used in research or for micro-manufacturing [10,11]. The morphology of dried specimen deposited using inkjet technologies is influenced by solvents with a specific surface tension which have an impact in the evaporation rate and the flow characteristics during the drying process [10]. Influences on the ink droplet spreading are also described in literature [12]. In common inks, surfactants are added to a water based dye for surface tension control [13]. Besides the surface tension, the viscosity of the liquid has a major influence in the droplet characteristics [13]. It is expected, that picoliter derived specimen prepared from aqueous standard solutions are affected by the same factors.

A comprehensive overview on nanoliter and picoliter printing with respect to TXRF in analytical chemistry is found in Hampel et al. [5] Compared to microliter derived residues with a diameter of *ca.* 1–5 mm [2], picoliter residues are way smaller with diameters in the range of *ca.* 5–200 μm depending on the cartridge type [2,8]. Residues derived from picoliter droplets (160 pL [14]) are obtained within seconds due to the fast drying process within tenth of a second [2]. The sample preparation was carried out at room temperature. It is not entirely clear how higher temperatures impact the morphology. Higher temperatures may favor particle-like specimen when the solvent evaporates before or at the impact of the droplet on the carrier. This intriguing but complex aspect was not subject to this study. To study instrumental performances and the influences of specimen characteristics, the droplets are deposited onto reflectors or substrates as single or multi element standards in aqueous solution with a defined pattern where the residues are having nearly the same size [4,9]. Prior studies have shown that the morphology of the picoliter printed residues on Si-wafers are comparable to those applied on quartz glass sample carriers (which were used in this work) and are having a spherical shape [5,6,9].

The analyte concentration in the droplet has an impact on the applied mass and therefore on the morphology [6]. Also a higher quiet time (the quite time is the time between two droplet ejections) leads to a higher concentration of the analyte in the droplet due to evaporation from the nozzles [5,9]. Higher masses are positively correlated with residue heights [9]. Additionally, the sample carrier roughness could have an influence on the wettability as well as the contact angle of the droplet on the sample carrier. For reducing the surface tension of the droplets and thus the contact angle the use of a water-soluble surfactant like Triton X-100 was used in this work. Certain surfactants are able to change the flow characteristics of droplets during drying to a Marangoni flow [15] that is also reported for droplets deposited using actual inkjet printing techniques with a combination of specific solvents [10]. Lowering the contact angle leads to a wider spreading of the droplets as they impact on the sample carrier surface [16,17]. By the addition of slightly volatile solvents like isopropanol, the evaporation rate and thus the specimen morphology can be influenced as well [17].

Static charges occurring on the silicon dioxide surface of the sample carrier further impact the film formation. Surface charges can have a major impact on the droplet contact angle and spreading. Both will also depend on the droplets surface charge. It is expected that droplets become statically charged when leaving the nozzles of the cartridge, *e.g.*, as in continuous inkjet printing systems [11,18]. Negative charges on quartz glass can occur by deprotonation of the silanol groups under contact with water. The negative charge density is a function of the pH-value and is positively correlated with the pH [19]. The cleaning process of the sample carriers may also induce static charges for the same reason. They were cleaned with basic and acidic cleaning solutions and with water at the end.

In general, the transfer and interaction at water/silicon-oxides interfaces are quite complex. When a water droplet gets in contact with a surface, negative charges are transferred from the surface to the droplet through electron and ion transfer [20]. The sample solutions used in this work are basic with pH values of 9–10, accordingly they are able to deprotonate the silanol groups. The simple handling of the sample carriers (*e.g.*, placing them in plastic petri dishes) may also induce static charges on the quartz surface. Techniques like electrowetting-on-dielectric also make use of electric fields. By applying an electric field to a conductive droplet the surface tension gets reduced resulting in droplet movement which is applied in microfluidic platforms [21]. Furthermore, on superhydrophobic surfaces, droplets are able to move along the surface charge density gradient [20].

In this study, for obtaining a small contact angle and improved spreading and preventing the movement of the picoliter derived droplets the sample carrier surface was not siliconized. The influence of a static eliminator and some other parameters on obtaining film-like morphologies was tested. In case the reflector surface (*e.g.*, due to Si–O-groups) and the droplets (due to strong basic conditions) are both negatively charged at the surface, a positive impact of charge elimination can be expected.

The aim of this work is to identify parameters and settings especially the influence of using charge elimination leading to film-like specimens of anionic ethylenediaminetetraacedic acid (EDTA) complexed solutions in basic conditions. The complexation with EDTA is necessary to keep the cations in a stable solution. It prevents them from adsorption on the cartridge wall surfaces. Stabilization using acidic conditions is not possible in this set up, it results in cartridge corrosion [5]. Hence, the complexing agent is a mandatory component of the sample solution which makes it very difficult to test the influence of it on the film formation. It can be concluded however from the studies presented here, that particle-like as well as film-like specimen can be obtained from anionic EDTA complexed solutions [4,5]. The determination of specimens being particle-like and film-like is solely done by the shape of the GIXRF measurements. However, according to calculations of von Bohlen et al. particle-like curves are obtained for specimens exceeding the coherence length of the excitation radiation which is usually several 100 nm. Typically, film-like GIXRF scans are obtained for sample heights of some single digit nm, *e.g.* 5 nm [22].

The relationship between the particle size or film height and the progression of the signal intensity during GIXRF measurements is described by Klockenkämper and von Bohlen [2]. When the sample is placed in the X-ray standing wave field (XSW) during an GIXRF measurement, the nodes and antinodes are penetrating the specimen. With increasing glancing angle, the number of nodes and antinodes increases while their thickness is decreasing. GIXRF can be used for the determination of the analytes particle size or the height of the analyte film, respectively. The angle dependent signal intensity of smaller particles, *e.g.*, 1 nm or thin films, shows a strong increase of nearly fourfold the post critical angle intensity just before reaching the critical angle, while sizes of about 100 nm are showing an oscillating intensity progression to the two- or threefold intensity [2].

Sparks et al. showed first grazing incidence X-ray fluorescence analysis of picoliter derived residues with regard to Si-wafer surface contamination control. In general particle-like and film like contamination samples are distinguished. The particle-like specimens show quasi-double excitation below the critical angle while thin films have a sharp peak close to the critical angle [6]. Besides the particle-like morphology there are also height effects visible if there is only a single residue [4]. Those height effects were studied by Till et al. with measurements and theoretical calculations on large residues [23]. Hence, the morphology of the sample has a strong influence on the angle-resolved intensity in GIXRF [2]. Fig. 1A visualizes theoretical GIXRF measurements for particle-like (blue scan) and film-like (red

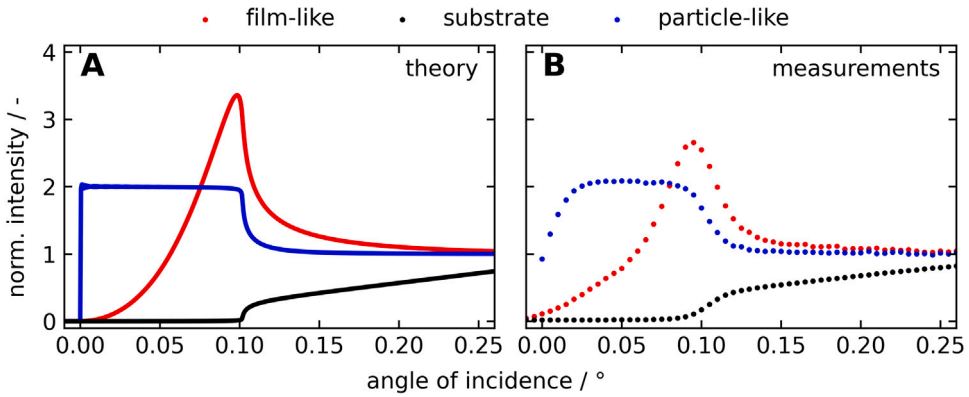

Fig. 1. Different morphologies in grazing incidence X-ray fluorescence analysis (Mo Kα = 17.5 keV, Si reflectors). Left: Ideal conditions (1 nm layer (film-like), 10 μm residue (particle-like), and bulk substrate) calculated according to literature [22,24–26]. Right: Non-ideal conditions from measurements of microliter derived specimens. (For interpretation of the references to color in this figure legend, the reader is referred to the web version of this article.)

scan) residues calculated according to literature [22,24–26] as well as real measurements in Fig. 1B.

The measurements show the same distinctive features as the simulations. Theoretical calculations are idealized with full excitation of the specimen on a perfect flat and smooth reflector using a parallel beam with no energy divergence. Non-ideal conditions are caused for example by: (a) real reflector's surface roughness [2], (b) the Gaussian shape of the beam, with slight divergence from being parallel [27], (c) the monochromator's energy divergence [28], (d) the specimen heights causes excitation by the beam below 0° [23], and (e) the specimen having an offset to the detector [4]. Many of these parameters can be addressed by software packages published by Ingerle et al. as well as Brigidi and Pepponi [29,30]. The instrument parameters can often not be changed and only the sample preparation can be optimized.

Hampel et al. have studied picoliter derived specimens with different patterns using GIXRF to learn about the pattern/morphology — signal relation. The GIXRF scans were performed with a parallel beam (using Goebel mirrors) and a more divergent beam from a focusing multilayer monochromator [4].

Von Bohlen et al. calculated different angle-dependent relative intensity profiles. For small sample heights in the range of 1–10 nm, the typical film-like profile was obtained [22].

Sample preparation techniques used for depositing thin layers in the micrometer or nanometer range include spin coating, physical and chemical vapor deposition [31]. During spin coating for example, a liquid solution is distributed on a substrate by rotation. The thickness of the resulting layer is thereby influenced by the speed of the rotation, the acceleration and the time. Also the characteristics of the liquid, the temperature and humidity are described in that review [31].

For performing quantitative analysis, a calibration which is converting the measured signal into a quantity is necessary [32]. Depending on the analytical method, the calibration can be carried out via an IS, like in (T)XRF [2,32] or via a calibration function using external standards [32]. With respect to TXRF it means that the internal standard concentration or mass need to be known or given to quantify the respective element(s) in the sample [2]. In contrast to the methods for depositing thin layers on substrates described above, picoliter derived specimen can be deposited with high reproducibility in mass in an user-defined pattern and can be used as a reference sample for quantitative analysis in TXRF measurements [5]. The goal of this study was to overcome the challenges in the preparation of film-like morphologies using picoliter drop on demand printing with aqueous sample solutions. Applying static charge elimination on the sample carriers, using additives, low concentrations and carefully selected printing parameters it is now possible to reliably deposit Ni thin films onto sample carriers which can be used in the future as a quantification standard for samples having the same morphology.

The sensitivity of an elemental line in TXRF is derived by the signal to concentration ratio, which is angle dependent, especially for film-like specimens. The normalized intensity progressions of film-like and particle-like morphologies differ significantly from one another and overlap at the iso-angle of ≈0.075° (see Fig. 2). This calibration problem has been addressed predominantly in semiconductor quality control. Traditionally, standard wafers coated with thin layers of Ni were used for calibration exhibiting the same angle dependent sensitivity as the wafer surfaces to be analyzed. The newer "Vapor Phase Deposition" strategy however resulted in a dried deposit, which often exhibited particle-like angle dependence [6]. A round robin comparing results on Ni-coated wafers, found sever deviations between using particle-like and film-like calibration standards. Deviations calibrating with matching morphologies were 7% and 5% while using particle-like calibration a positive bias of 35% was found. These deviations were observed although the determination was performed at the iso-angle [33]. The glancing angle for TXRF measurements described commonly in literature is equal to 50%–70% of the critical angle of the sample carrier material (here, ϕ_{crit}(quartz,17.5 keV) = 0.1°) [2,34]. In a set up like the one used here (featuring a Goebel mirror for molybdenum Kα) the signal will differ 7%–52% between 0.07° and 0.05°, respectively. Haberl et al. using an Atomika 8010 instrument identified an uncommon morphology, however still particle-like appearance of the Rb analyte in a multi-element fly ash sample as the reason for an underdetermination of up to 20% [35]. The deviations between particle-like and film-like specimens may become less severe by increasing the divergence of the primary beam. However, it was shown that significant differences remain [36].

In this study, we focused on establishing a robust procedure for film-like specimen formation. In future work film-like external calibration standards will be applied to study samples like wafers and aerosols. This will require additional effort in method validation, considering, *e.g.*, lateral dimensions of the samples and the detector field of view. This will go beyond the scope of the study presented here.

Fig. 2 indicates in grey the typical angle range of TXRF measurements for both, film- and particle-like morphologies. Laboratory TXRF devices may not always have the capability of angle scanning and the measurement position is set to the maximum intensity in general of a particle-like calibration standard and films are usually not considered. Under those prerequisites an external calibration with film standard is necessary in order to prevent quantification bias due to the position deviation.

In the future this capabilities need to be evaluated for other elements. Additionally, it will be possible to imitate real samples like "coffee rings" through combining particle-like and film-like residues to investigate their influences in TXRF measurements. The determination of a specimen being particle-like or film-like is solely done by the angle

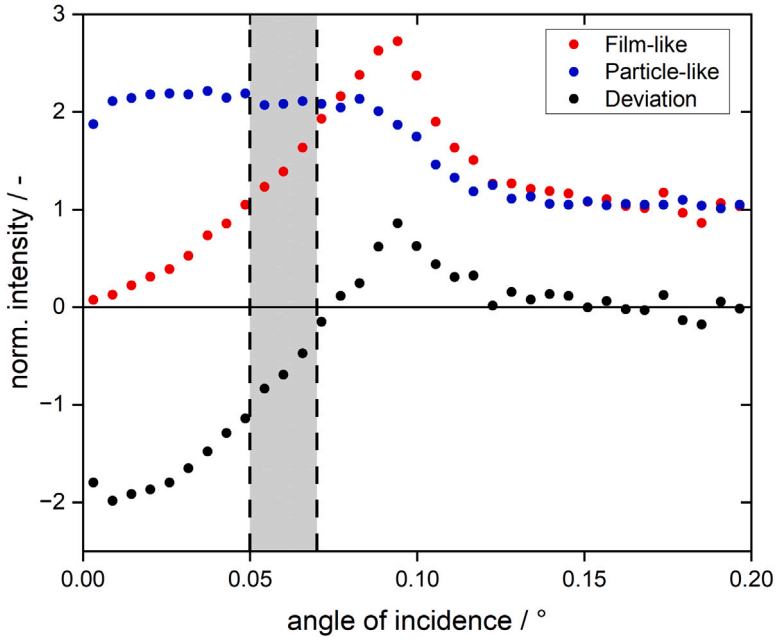

Fig. 2. Deviations (black) between the normalized intensities of film-like (red) and particle-like (blue) GIXRF measurements. Possible TXRF incidence angles 0.05°–0.07° [2,34] are illustrated within the grey marking. The film-like and particle-like curves intersect at an iso-angle of ≈0.075°. (For interpretation of the references to color in this figure legend, the reader is referred to the web version of this article.)

dependent intensity profile. It is strongly supported by theory [2,22] and experimental evidence [6]. True *e.g.* spin coated films [6] and single digit nm particles [22] both show film-like angle dependence of the signal. With respect to this study, the presence of the organic ligands has yet unknown influence on the shape. Therefore atomic force microscopy (AFM) was used as a second method to probe the shape of the residues.

2. Materials and methods

2.1. Chemicals and materials

Single element Ni, Co, Ga and V ICP stock solutions (1 g L^{-1}, Roti®Star, Carl Roth, Karlsruhe, Germany), ethylenediaminetetraacedicacid (EDTA) (99%, Alfa Aesar, Haverhill, USA), 10% ammonia solution (pure, Carl Roth, Karlsruhe, Germany), Triton X-100 (pure, SERVA Electrophoresis, Heidelberg, Germany), silicone solution in isopropanol (SERVA Electrophoresis, Heidelberg, Germany), isopropanol (for analysis, Merck KGaA, Darmstadt, Germany), Fluorescein (for analysis, Riedel de Haën AG, Seelze, Germany), 40% hydrofluoric acid (for analysis, Carl Roth, Karlsruhe, Germany) and 69% Nitric acid (supra, ROTIPURAN®, Carl Roth, Karlsruhe, Germany) were used for preparation. Ultrapure water (≈0.055 μS cm^{-1}, Purelab Flex 4, Elga Lab Water, High Wycombe, United Kingdom) was used for dilutions. The sample solutions were deposited with C6602A cartridges (HP, Palo Alto, California, United States of America) with a droplet volume of ≈160 pL [14]. All preparation steps were carried out in laminar flow boxes (Cruma 870 FL, Diantech Solutions S. L., Barcelona, Spain and FBS 75, Spetec GmbH, Erding, Germany).

2.2. Sample solutions and internal standardization

A 60 mmol L^{-1} EDTA stock solution was prepared from 0.6967 g EDTA, 3.2 mL 10% ammonia solution, and filled to a total volume of 40 mL with ultrapure water. To obtain the ≈0.0067% (w/v) Triton X-100 stock solution, ≈2.5 μL Triton X-100 were diluted with 40 mL ultrapure water. The Ga stock solution was diluted in two steps with Nitric acid and ultrapure water to gain the end concentration of 0.1 mg L^{-1}. The Vanadium standard solution was diluted to 0.5 mg L^{-1} in two steps as well.

Solutions for contact angle determination as well as picoliter printing on Si-wafers were prepared in different concentrations (10, 50, 100, 200, 300, and 600 mg L^{-1}) from the Ga standard, EDTA stock solution, 10% ammonia, and ultra-pure water according to Hampel et al. [5]. The 10 mg L^{-1} solution was diluted (0.1, 0.5, 1, 2, 3, and 6 mg L^{-1}) with 5 vol% of 10% ammonia for the microliter derived specimens in basic solution. Acidic solutions of the same concentration were prepared from the Ga standard with 5 vol% of 69% nitric acid.

100 μL of the Ni stock solution were mixed with 30 μL of the EDTA stock solution, 30 μL 10% ammonia solution, either ≈1000 μL of the Triton X-100 stock solution or 1000 μL isopropanol if any of those additives were used and filled up to 10 mL with ultrapure water for pL printing.

For better visibility of the residues in the AFM camera image, fluorescein was mixed with 10% ammonia solution and ultrapure water to a 0.3 mol L^{-1} solution and then added to the 10 mg L^{-1} Ni solution to gain an end concentration of fluorescein, present as the ammonium salt of 5.9 mmol L^{-1}.

2.3. Picoliter drop on demand printer

To enable the deposition of user defined patterns, the reflectors were placed on the xyz-stage of the picoliter drop on demand printer based on a HP-printing cartridge and a micro controller. The picoliter printer as well as the precise printing procedure is described by Hampel et al. [5]. The printing parameters include the quiet time (time between two droplets), the distance between two droplets and the number of deposits in a given pattern. The printing pattern are consisting of several pixels. One deposit is usually formed by spotting one droplet per position (pixel), however in the 16 × 16 pattern the number of droplets per point were increased to three. The number of droplets being applied in total in a pattern is obtained by multiplication of the number of droplets per position and the number of deposits (pixels). The 16 × 16 pattern for example consist of 216 deposits (pixels) so the deposition of three droplets per position results in 648 droplets in total. The parameters of this study are shown in Table 1.

Table 1
User defined printing patterns with the respective printing parameters used for deposition.

Pattern	(a)	(b)	(c)
Droplets/position	1	1	3
Quiet time [s]	0.4	0.3, 0.5, 1.0	0.5
Distance between two droplets [µm]	200	200	200
Number of deposits	400	676	216
Number of droplets	400	676	648
Pattern size [mm]	4 × 4	5 × 5	∅ = 3

The two different patterns (b) and (c) described in Table 1 are used for the investigations in the film formation of aqueous Ni solutions with different printing parameters, additives and with regard to the surface quality of the quartz glass reflector. Described by Hampel et al. the intensity profile of the Bruker S4 T-Star® detector field of view (FOV) is Gaussian distributed and therefore the measured intensity of the printed patterns are decreasing with increasing distance from the detector FOV. The further the printed residues are placed apart from the center of the sample carrier the less respective intensity can be captured by the detector which is leading to an underestimation so that printing patterns cannot be infinitely large in diameter [4]. The respective sample carriers were not siliconized before usage improving the film formation process. For the quantification of those patterns, separate quantification samples were prepared on previously siliconized sample carriers where 10 µL of a silicone solution in isopropanol was applied (SERVA Electrophoresis, Heidelberg, Germany). After drying, a defined number of droplets was deposited as a single residue in the middle of the quartz glass carrier with the same quiet time which was used for the respective samples as the quiet time has an influence on the signal intensity and thus on the applied mass [9]. The quiet time is an adjustable printing parameter and describes the time that passes between the release of two single droplets. During that time, the solvent at the nozzle evaporates which leads to a higher element concentration in the droplet and thus to bigger residues and higher element masses in the respective deposits [9]. 10 µL of the 0.1 mg L^{-1} Ga solution (m_{Ga} = 1 ng) or 10 µL of the 0.5 mg L^{-1} V solution (m_V = 5 ng) was then pipetted manually on that deposit and dried under infrared light resulting in particle-like morphology for both, analyte and internal standard.

2.4. TXRF and GIXRF measurements

Two laboratory grazing incidence X-ray fluorescence (GIXRF) devices were used. Specimens on Si-wafers (675 µm thickness) were measured with a custom-built setup by Brigidi and Pepponi [30]. A Phoenix multi-purpose diffractometer (TNX Srl) with Mo X-ray tube (40 kV, 30 mA, Kα = 17.5 keV) and multilayer optics (AXO Dresden) were used together with a silicon drift detector (Ketek). The detector was placed perpendicular to the incident beam and specimens were placed manually under the detector. GIXRF spectra were taken with 60 s exposure per step ($\Delta\phi$ = 0.005°) for microliter derived specimens. Picoliter printed samples were measured with 600 s dwell time.

Specimens on quartz glass carriers (B&M Optik, Limburg, Germany) were measured with a Bruker S4 T-Star® (Bruker Nano GmbH, Berlin, Germany) using an air-cooled Mo X-ray tube (50 kV, 1 mA, Kα = 17.5 keV) with a 60 mm^2 silicon drift detector. For examining the morphology of the samples, GIXRF measurements were performed using the non-focusing Goebel mirror optics with a measurement time of 1000 s per step ($\Delta\phi \approx 0.005°$). The angle dependent intensities were normalized on the mean of the last three measurement points. Error intervals were determined using error propagation from the errors of the counting statistics. Offsets of the motor position during acquisition were corrected to the critical angle of silicon (ϕ_{crit} = 0.1°, quartz, 17.5 keV) [2]. The calibration of the motor positions to the angles was performed by determination of critical angles of different materials as described by Till [37]. To quantify the respective Ni masses quantification samples were measured with total reflection X-ray fluorescence for 1000 s using a focused multilayer monochromator and the net intensities were corrected with the blank values which were measured with the same measurement parameters. Therefore, the respective element counts of the cleaned and siliconized sample carriers (blanks) were subtracted from the element counts of the respective quantification sample carrier. For both measurements the sample carriers are placed in the exact same measuring position. Count rates of the elements of interest for the blank sample carriers were in the two to low three digit range. On the quantification samples count rates in the four to five digit range were measured for the elements of interest.

The evaluation of TXRF and GIXRF spectra was done using PyMca version 5.4.2 [38]. Quantification of the Nickel masses (m_{Ni}) are calculated with Eq. (1) using the net intensities of Ni (N_{Ni}) and the internal standard (N_{IS}), the mass of the internal standard (m_{IS}) instead of its respective concentration and the manufacturer given relative sensitivities of Ni (S_{Ni}) and the internal standard (S_{IS}) [2]. 1 ng Gallium or 5 ng Vanadium were used as internal standard. With the applied 1 ng Gallium as internal standard (S_{Ga} = 1) Eq. (1) can be simplified.

$$m_{Ni} = \frac{N_{Ni} \cdot m_{IS} \cdot S_{IS}}{S_{Ni} \cdot N_{IS}} = \frac{N_{Ni} \cdot 1\ ng}{S_{Ni} \cdot N_{Ga}} \quad (1)$$

After performing a Grubbs outlier test on the respective 6–8 quantification samples [39,40], the analyte masses were averaged and given in nanogram (ng) with the 95% confidence interval. For the Grubbs outlier test, the standard deviation based on a sample from a population (n-1 method) was used [40].

2.5. Contact angle determination

For the contact angle determination an Edmund optics EO-0413M camera (752 × 480 px, monochrome, 8 bit) with small objective was used together with a manual translation stage to position the sample into focus. A 1.5 µL droplet was placed with a microliter pipette onto the surface of the reflector and an image is taken. The process is done with at least six replicas per solution. Si-wafers (675 µm thickness) were used without pretreatment for the native silicon oxide. A hydrofluoric acid dipping (2 w%) of the same batch of wafers yielded the freshly etched silicon.

Data processing was done within ImageJ [41] with the Drop Analysis plugin [42,43]. Basic splines (B-splines) are fitted onto the droplet (see Figure S1 in supplementary) and the contact angles are derived from the B-splines. After a Grubbs outlier test the contact angles are noted as mean values with 95% confidence interval.

2.6. Static eliminator

The static eliminator AD 1683 (A&D Company Limited, Oxfordshire, United Kingdom) was placed at a distance of ≈20 cm from the middle of the sample carrier which is placed on the xyz-stage of the picoliter printer as indicated in Fig. 3.

The eliminator was running at least 4 s before starting the printing procedure and was left running during that. The preparation of the quantification samples was done without using the static eliminator.

2.7. Atomic force microscopy

Residue shapes and the roughness of the sample carriers were determined using the atomic force microscope NX12 with the Smartscan™ software version 2.0 RTM2d (2024-9-12) (Park Systems, Suwon, Korea). A silicon AC200TS cantilever (150 kHz resonance frequency and spring constant of 9 N m^{-1}) with 7 nm tip radius (Olympus, Tokio, Japan) was used in non contact mode at ambient conditions. The

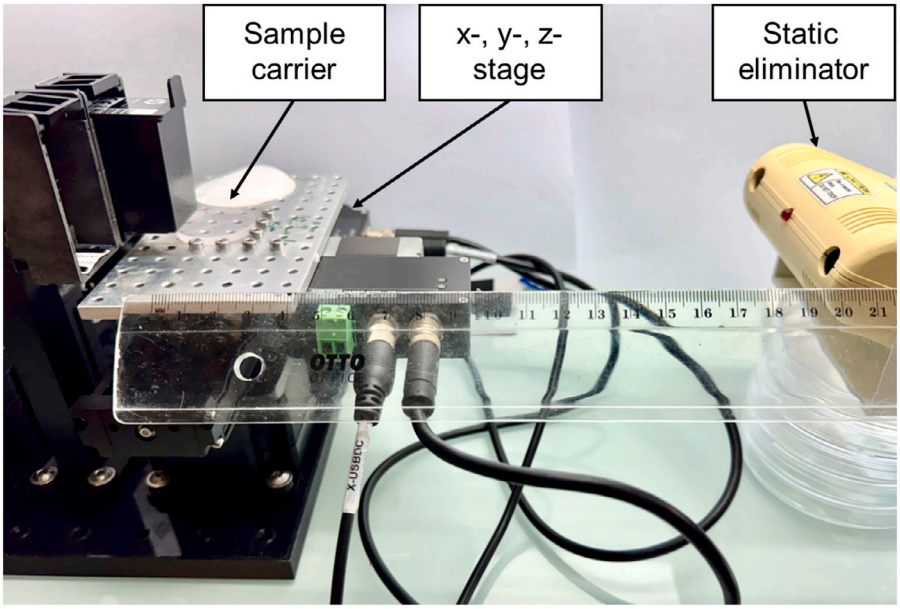

Fig. 3. Experimental setup consisting of the picoliter printer (left) and the static eliminator placed at a distance of 20 cm (right).

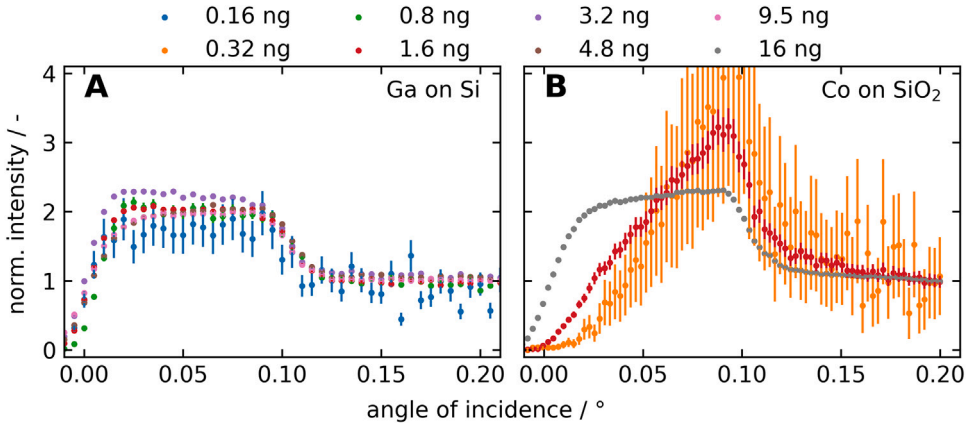

Fig. 4. GIXRF of picoliter droplet derived residues on freshly etched silicon (left side) and quartz glass carriers (right side). According to Ref. [36]. (For interpretation of the references to color in this figure legend, the reader is referred to the web version of this article.)

resolution is given by the images (1024 × 1024 px) and the scanned area. For 50 µm × 50 µm areas and 90 µm × 90 µm the resolutions are given with 49 nm and 88 nm, respectively. The measured data were evaluated using a combination of Gwyddion [44,45] version 2.67.20250131 and version 2.66 and XEI version 5.2.0.Build1 (Park Systems, Suwon, Korea). Before starting the evaluation process, the captured z-height forward pictures of the sample surfaces were three point leveled and treated in the way that the facet level function was applied, the rows were aligned using the median method and if necessary, the horizontal error lines were corrected. In the end, the minimum height was set as the zero value and the Gwyddion.net color code in combination with the automatic color range tool was used for better visibility. The roughness calculation is done by the program using Eq. (2) [44–46].

3. Results and discussion

3.1. Influences of the delivered analyte mass on the film formation

The influence of printed masses on film-like residues formation have not been studied very detailed yet. Sparks et al. [6] have shown that Ni film-like specimens occurred printing deposits of 0.0225 pg while 2.25 pg per deposit yielded particle-like samples on clean Si-wafers. In our previous studies residues were obtained on siliconized reflectors, these hydrophobic surfaces promote particle-like morphology [4,5]. Tsuji et al. gained a hydrophilic surface promoting films by treating glass with a Helium atmospheric pressure plasma jet. The modification of the surface obtained a reduction of the contact angle between the substrate and the droplet [47]. Hence, clean more hydrophilic surfaces should be preferred. Freshly etched Si-wafers are hydrophobic and also promote the formation of particle-like morphologies. Here we study a

Table 2
Contact angles of water and Ga in acidic conditions as well as EDTA complex using 1.5 µL droplets on freshly etched silicon and native silicon oxide. The contact angles are noted as mean with the 95% confidence interval (CI). According to Ref. [36].

Liquid	θ_c ± CI(95%) [°] freshly etched silicon	θ_c ± CI(95%) [°] native silicon oxide
water	70.3 ± 2.0 (n = 36)	50.6 ± 2.6 (n = 24)
6 mg L^{-1} Ga acidic	70.5 ± 3.9 (n = 12)	52.8 ± 2.7 (n = 22)
6 mg L^{-1} Ga-EDTA	67.9 ± 2.8 (n = 12)	45.0 ± 2.1 (n = 24)
100 mg L^{-1} Ga-EDTA	54.7 ± 6.0 (n = 12)	52.7 ± 4.9 (n = 24)

wide concentration range from 0.4 pg to 40 pg per droplet delivered with the picoliter printer (residues were derived using a 20 × 20 pattern (4 × 4 mm)) on an etched Si-wafer and on untreated quartz glass carriers. Subsequent GIXRF scans are shown in Fig. 4A for the etched surface and B for the quartz reflectors. On the etched Si surface particle-like residues were achieved over the whole concentration range indicating the good reproducibility of the morphology. The smaller droplets tendency of forming films is drastically reduced at high contact angles. The surface charge may also play a role, but the impact of the HF etching on the contact angle dominates the formation of particle-like residue. Printing similar concentrations on untreated quartz glass carriers, a strong dependence of the concentration onto the morphology is visible (see Fig. 4B). With small concentrations, *i.e.* 0.8 pg and 4 pg per deposit, film-like and close to film-like residues are obtained, while with increasing mass the particle-like fraction increases until quasi-double excitation is visible. In comparison microliter droplet derived residues show no trend of the morphology depending on the deposited mass (see Figure S2).

All residues consist only of a single droplet per point. By this procedure only the interaction of the droplet with surface remains and can be probed. The most critical parameter influencing the morphology is the contact angle between liquid and surface and the surface roughness has also minor impact. The contact angle (see Figure S1) was probed for water, Ga-EDTA complex with high (100 mg L^{-1}) and low concentration (6 mg L^{-1}) as well as Ga in acidic solution (6 mg L^{-1}). The four solutions cover not only picoliter printing but also microliter deposition for regular liquid sample preparation. Table 2 shows the contact angle of the mentioned solutions on freshly etched silicon as well as native silicon oxide layers. The Ga standard was used here to accommodate interference present in one of the GIXRF spectrometers [30]. Cobalt and nickel were tested together with different 3d metal ions for their film formation capability. The EDTA complex stability constants of these three elements are quite similar ($logK_{Ga}$ = 20.3; $logK_{Co}$ = 16.3; $logK_{Ni}$ = 18.6) and in the middle of those from 65 elements printable as has been shown previously [5,48]. Additionally, Ni is the standard element in silicon wafer quality control, as it exhibits favorable diffusion in silicon and stays at the wafer surface. It has become the standard element in TXRF in general. Hence Ni was used for all studies applying the static charge elimination.

The expected contact angles for water are met on both surfaces with 70.3 ± 2.0° on silicon as well as 50.6 ± 2.6° and are comparable to literature data from Hermansson et al. and Yang et al. [49,50]. The prepared Ga-EDTA solutions were optimized for their printability requiring sufficient amounts of ammonia to prevent adsorption effects. In the 100 mg L^{-1} Ga-EDTA solution there is *approx.* six times more ammonia than in the 6 mg L^{-1} Ga-EDTA solution, which may also influence the contact angle. The contact angle on freshly etched silicon and native silicon oxide are equal indicating changes of the surface, *e.g.*, (a) etching or (b) re-oxidation and subsequent negative surface charges. While ammonia acts mostly as an etchant [51–53], the interplay of ammonia and EDTA may result in oxidation rather than etching similar to hydrogen peroxide/ammonia cleaning processes [51]. On microscopic level the high elemental concentration in the deposited residue will yield particle-like residues and the film formation is unlikely. It is obvious that film formation on etched surface cannot be achieved easily, hence all following preparations were performed on native quartz reflectors.

The GIXRF scan shapes are classified according to their appearance. The shape form is assigned according to the reference shapes shown in Fig. 5, with A being completely particle-like (blue), B being a mix between film-like and particle like (orange), C being nearly film-like (green) and D being completely film-like (red). The color code will be applied to the GIXRF scans for optical classification of the sample morphology. In the last two columns of Table 3 the GIXRF scan of each specimen according to this classification is given. All performed GIXRF measurements evaluating the influence of different parameters on the Ni film-like morphology are displayed in Fig. 6. The respective sample numbers can be assigned to the tested parameters shown in Table 3. In the following sections the influence of the surface roughness, additives and finally of the elimination of static charges for producing film-like residues is discussed. It is shown, that on common quartz glass carriers, the combination of using an additive and static elimination makes the production of film-like specimens very reliable.

3.2. Surface quality

In the previous section it became clear that the hydrophilic character of a surface has a major influence on the film-like specimen formation. In the following, untreated quartz glass carriers with surface characteristics (contact angles from 45–53°) as shown in Table 2 were used. These carriers are common in TXRF analysis [2]. The surface roughness of the quartz glass carriers need to be lower than 5 nm within an area of about 1 mm^2 to be able to totally reflect the incoming X-ray beam according to theory [2]. It is assumed that rough surfaces can also lead to more particle-like specimens, as scratches on the surface tend to pin the contact line of the liquid during the drying process [3]. Using atomic force microscopy, the sample carriers where measured in non contact mode for determining the respective average roughnesses R_a according to Eq. (2) where N represents the evaluation length and r_j the average deviation from the mean line [46]. Therefore, the center of the sample carrier was placed underneath the cantilever to probe an area of 50 μm × 50 μm which is considered as representative for the whole sample carrier. Vertical and horizontal lines where measured within the probed area. The indicated sample carrier roughness's below are *approx.* the highest measured values.

$$R_a = \frac{1}{N} \cdot \sum_{j=1}^{N} | r_j | \tag{2}$$

The roughnesses of a sample carrier set consisting of 24 quartz glass discs were determined within the range of 0.2 nm to 1.5 nm and are therefore even smaller than the recommended 5 nm given in the literature [2]. Within the measured range, the influence of the sample carrier roughness can be neglected. The respective surface roughness is given in Table 3 (sample No. 9–26), showing that the roughness has no remarkable influence on the GIXRF scan shape (see Fig. 5). The specimen on the roughest carriers with 1 nm roughness, *i.e.* sample 11 and 13 both exhibit a film-like shape (D-shape according to Fig. 5). For GIXRF scans see Fig. 6.

3.3. Additives

Additives like Triton X-100 are frequently used in TXRF [1,16]. It has been shown that they can improve the repeatability by means of lowering the relative standard deviations for samples with high saline concentrations [54] and preventing slurrys from aggregation in certain cases [1]. Additives in pL applications are not very common but are used to lower the contact angle between the printed droplets and the sample carrier in this work. For examining the influence of different additives, a Triton X-100 solution (end concentration in the sample solution ≈0.00067% (w/v); sample No. 12 , 15 and 23) and isopropanol (end concentration in the sample solution = 10 vol%; sample No. 16, 17), were chosen. The respective angle scans can be seen in Fig. 6. For comparison, samples with no additives were also prepared (sample No. 9, for GIXRF scan see Fig. 6.).

A 26 × 26 px square printing pattern was used. Only the sample No. 15 and 17 with Triton X-100 and isopropanol exhibited a very close to film-like GIXRF scan (C-D) (see Fig. 6.), all the other samples showed either a completely particle-like scan (A) (No. 9 and 16) as well as in-between shapes, *i.e.* No. 12 and 23, with both C-shape. The masses per deposit were quite similar and did not have a notable influence on the GIXRF scan. They were in the range of 0.88 pg (sample No. 16, shape A) to 1.4 pg (sample No. 12, 15 and 23 – C and C-D shape). The data is given in Table 3.

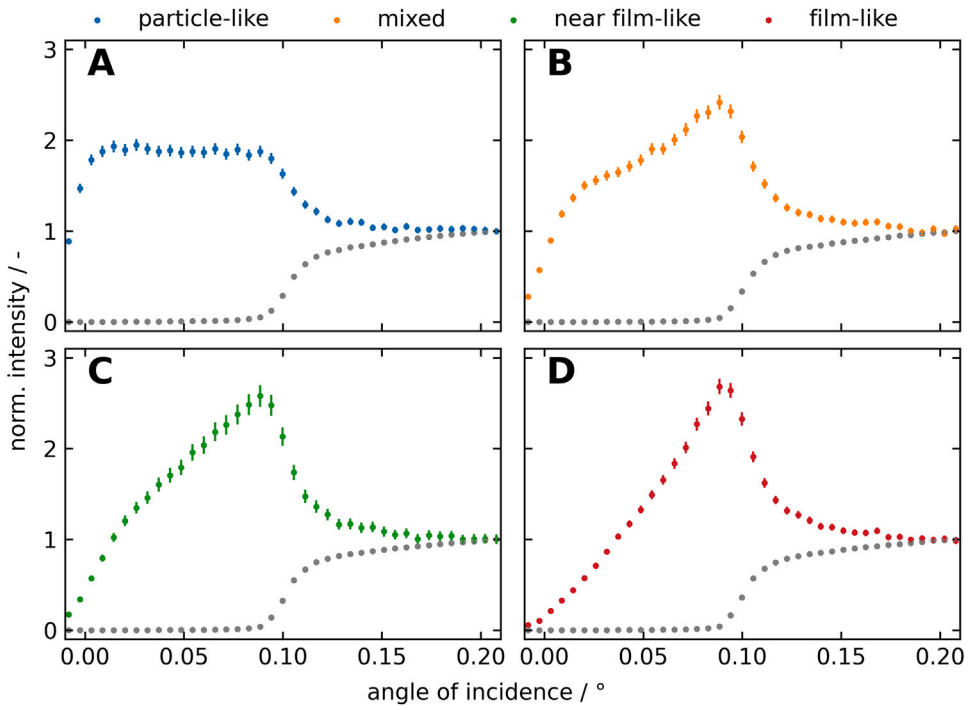

Fig. 5. Classification of GIXRF scan shapes with A being completely particle-like and D being completely film-like and B and C being near film-like and a mixed appearance. The substrate Si is illustrated in grey, respectively. (For interpretation of the references to color in this figure legend, the reader is referred to the web version of this article.)

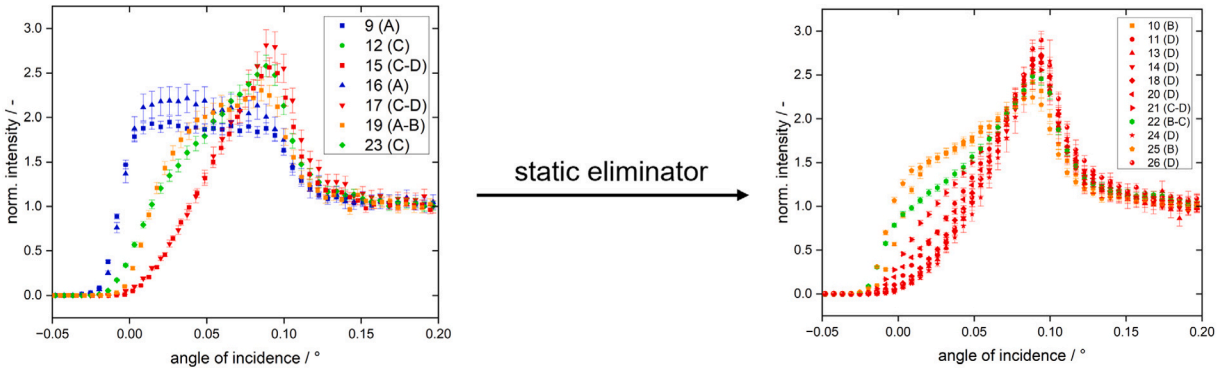

Fig. 6. Comparison of GIXRF measurements with and without static elimination. The samples are named according to Table 3. The respective scan shapes (A–D) are noted behind the sample numbers and the respective color code is applied. (For interpretation of the references to color in this figure legend, the reader is referred to the web version of this article.)

3.3.1. Multiple printing

The quiet time and the number of droplets deposited per position can be used for having control over the applied mass [5] of Ni onto the sample carriers. The mass can also be influenced by the relative humidity where a lower humidity is leading to a higher element count rate and to larger residues [9]. External conditions, *e.g.* the temperature, also have a remarkable influence on the drying procedure of droplets and thus on the homogeneity of the specimen [5]. The correlation of the temperature with the film formation is part of further tests and will not be discussed in this publication. However, the influence on spotting multiple deposits at the same position was tested.

Printing several droplets on top of each other may lead to a higher dried specimen than single printed ones. Here, in total *ca.* 4 pg were delivered with three droplets applied per position in a 16 × 16 pattern. Triton X-100 was used as an additive (sample No. 19). The angle dependent intensity progression is close to a completely particle-like shape (between A and B, see Fig. 6.). The same mass delivered in one deposit (see Fig. 4, 4 pg per deposit red dots) exhibited a film-like scan (D).

3.4. Elimination of static charges

In the previous section it was shown that reducing the delivered mass is an important factor for film-like specimen formation and also the additive is important. Nonetheless, the specimens often exhibit mixed behaviors. The introduction of static elimination as an additional parameter leads to a very reliable production of film-like residues.

Printing parameters that did not lead to film morphologies before can now be varied in a certain range for the respective additives to create user defined nickel films. For example sample No. 11 without any additives shows a film-like shape, being printed using static elimination. Nonetheless, without additive the reliability for obtaining a film is lower (*i.e.* sample No. 10 has a B shape). All samples with additives either Triton X-100 or isopropanol show a film-like behavior (sample No. 13, 14 and 18) when static charges are eliminated. The masses

Table 3
Overview of all samples with parameters and GIXRF scan shapes without (1) and with (2) the use of the static eliminator.

No.	Roughness [nm]	Mass/deposit [pg]	Total mass [ng]	Additive	Shape 1	Shape 2
Gallium	On etched Si-wafer	20 × 20 pattern				
1	–	0.4	0.16	–	A	–
2	–	2	0.8	–	A	–
3	–	4	1.6	–	A	–
4	–	8	3.2	–	A	–
5	–	24	9.5	–	A	–
Cobalt	All following on Quartz glass	20 × 20 pattern				
6	–	0.8	0.32	–	D	–
7	–	4	1.6	–	C	–
8	–	40	16	–	A	–
Nickel		26 × 26 pattern	Test additives			
9	0.4	–	–	–	A	–
10	0.5	2.3	1.54	–	–	B
11	1	2.3	1.54	–	–	D
12	0.5–0.6	1.4	0.97	Triton X-100	C	–
13	1	1.2	0.79	Triton X-100	–	D
14	0.5–0.8	1.9	1.26	Triton X-100	–	D
15	0.2–0.3	1.4	0.97	Triton X-100	C-D	–
16	0.2–0.3	0.88	0.59	Isopropanol	A	–
17	0.2–0.3	0.94	0.63	Isopropanol	C-D	–
18	0.2–0.3	1.9	1.28	Isopropanol	–	D
Nickel		16 × 16 pattern	3 × droplets			
19	0.8–1.2	4.2	0.93	Triton X-100	A-B	–
20	0.5–0.6	5.7	1.21	Triton X-100	–	D
21	0.1–0.2	5.7	1.23	Isopropanol	–	C-D
22	0.1–0.2	6.9	1.48	–	–	B-C
Nickel		26 × 26 pattern	Same carrier			
23+24	0.5–0.6	1.4+1.2	0.97+0.79	Triton X-100	C	D
Nickel		26 × 26 pattern	Quiet time test (1 s)			
25	0.6–1.0	2.04	1.38	Triton X-100	–	B
26	0.3–0.5	2.04	1.38	Triton X-100	–	D

per deposit being 1.2 and 1.9 pg, respectively. Even the samples with 3 × printed deposits and masses of 5.7 pg obtain a film-like character with static elimination (sample No. 20, D shape and sample No. 21, C-D shape). When using the same sample carrier and Triton X-100 as an additive it is shown that with static elimination a film-like GIXRF scan D is obtained however not without the elimination (C shape) (see Fig. 6). All results are shown in Table 3.

3.5. Residue shape

It would be very interesting to have detailed information on the film-like dried residue dimension. Unfortunately, it was not possible to identify the deposits with atomic force microscopy. Through the camera image (839 μm × 629 μm) of the atomic force microscope the sample residues are hardly visible which complicates the correct positioning of the cantilever before starting the measurement. To overcome that problem, a fluorescein solution (end concentration in the sample solution 5.9 mmol L^{-1}) was added.

In Fig. 7 the shape of the film-like deposits printed in the 26 × 26 px square pattern with one droplet being applied per position can be seen. With fluorescein being used as a coloring agent, the film is visible as a combination of ring shaped residues and a wavy structure which covers the printed area. The GIXRF scan is also showing a film formation with a noticeable concave increase of the normalized intensity before reaching the critical angle and can be seen in Fig. 8. The addition of fluorescein seems to improve the film formation.

The heights of the ring shaped residues are varying from ≈5–60 nm and the diameter from ≈35–50 μm. The edges of the wavy structures are ≈30–120 nm high.

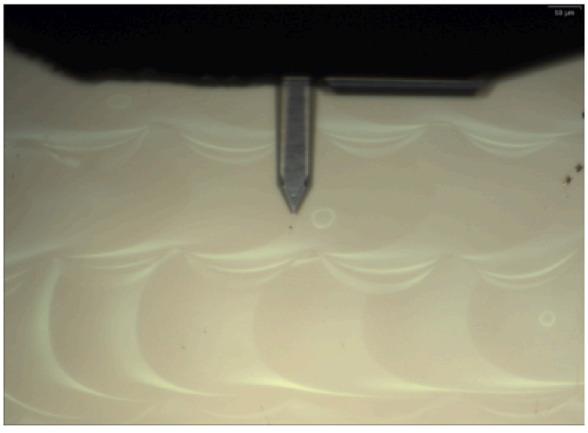

Fig. 7. Camera image (839 μm × 629 μm) capturing the residue shape of a 10 mg L^{-1} Ni solution with Triton X-100 as an additive and 5.9 mmol L^{-1} fluorescein solution with film morphology printed with one droplet per position and a quiet time of 0.5 s in a 26 × 26 px pattern. (For interpretation of the references to color in this figure legend, the reader is referred to the web version of this article.)

Nevertheless, the samples with the different additives without fluorescein were measured as well.

The AFM measurements of the actual printed sample solutions without fluorescein are not showing the wavy structures.

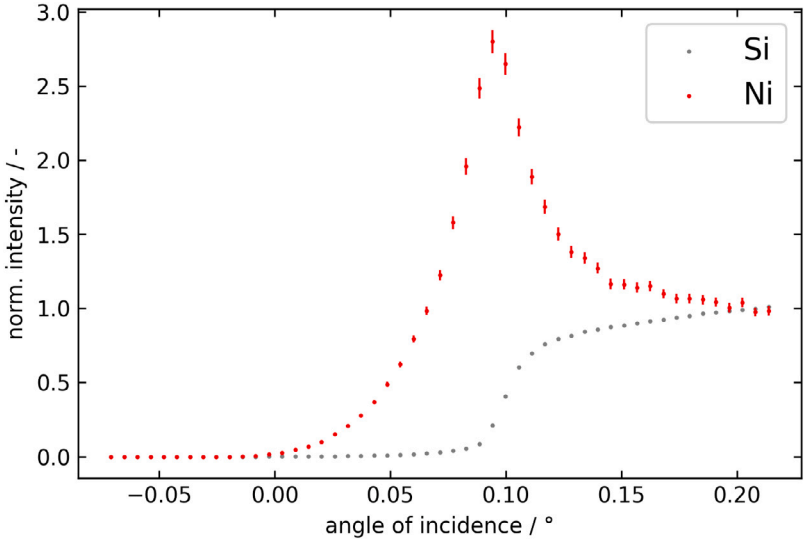

Fig. 8. GIXRF measurement of a 10 mg L^{-1} Ni solution with Triton X-100 as an additive and 5.9 mmol L^{-1} fluorescein solution printed with one droplet per position in a 26 × 26 px pattern with static elimination (D shape). (For interpretation of the references to color in this figure legend, the reader is referred to the web version of this article.)

It is obvious that the shapes of the residues are dominated by fluorescein. Its addition increases the heights and diameters which is not surprising as its concentration is *approx.* 200 times higher than Ni's in the sample solution. The AFM can be used to determine the shape, height and diameters in the sub nm range but it is not able to provide information about the elemental composition of the residues. The results from the AFM measurements of the fluorescein free specimen are available in the supporting information (Figures S3 - S5).

4. Conclusions and outlook

It could be shown that static charges have a strong impact on the film formation behavior which means that the elimination of static charges are favoring a better and more reliable film formation. Also the influence of different additives in combination with different printing parameters were evaluated.

Without static elimination, the morphology of the residues was mostly particle-like and a mix between film-like and particle-like, in few occasions film-like specimen were obtained but not reliable according to GIXRF measurements. The best results without eliminating static charges on the sample carrier were achieved using isopropanol with a 0.5 s quiet time and 1 droplet per position or Triton X-100 and 1 droplet per position. For Triton X-100, 0.3 s and 0.5 s quiet times were tested, whereas only the experiment using 0.5 s is shown (sample No. 15). However, these conditions did not always reproduce film-like specimen.

After eliminating static charges present on the quartz glass sample carriers, it was possible to create a standard procedure for producing film-like behavior reliably. The most promising results were gained using Triton X-100 as an additive (≈0.00067% (w/v)) in combination with eliminating static charges. It is possible to print residues with film morphology using quiet times of 0.3 s, and 0.5 s. Even printing three droplets on top of each other was providing film-like specimens. Quiet times of 1 s using Triton X-100 lead to a film-like specimen (D-type) and a B-type specimen. As mentioned before it is assumed that the quiet time mainly influences the delivered mass per droplet. The masses in sample No. 25 and 26 are quite low with 2.04 pg per deposit, so the longer standing time may also have an additional unknown effect. Isopropanol used as an additive is also leading to film-like morphologies by applying one droplet per position and a nearly film-like morphology by multiple printing. Using no additive is leading to no reliable results.

According to the tested parameters, Triton X-100 was found to be working most reliably in combination with the static eliminator. The now optimized standard procedure is leading to an improvement in film formation with reproducible results. Even GIXRF measurements with higher organic amounts (mass of fluorescein *approx.* factor 200 higher than mass of Ni) are showing a film-like character. However, the visualization of the residues using Ni and fluorescein cannot be extrapolated to the Ni films for residue shape estimation due to the high dominating mass of the coloring agent.

More investigations need to be done characterizing the shape of the specimen with techniques which can also visualize the element distribution on the sample carrier. In this way the sample residues can be clearly identified.

CRediT authorship contribution statement

Franziska Sand: Writing – review & editing, Writing – original draft, Visualization, Validation, Methodology, Investigation, Formal analysis, Conceptualization. **Sven Hampel:** Writing – review & editing, Writing – original draft, Software, Methodology, Investigation, Formal analysis, Conceptualization, Visualization. **Giancarlo Pepponi:** Writing – review & editing, Resources. **Ursula Elisabeth Adriane Fittschen:** Writing – review & editing, Writing – original draft, Resources, Project administration.

Declaration of competing interest

The authors declare the following financial interests/personal relationships which may be considered as potential competing interests: Ursula Elisabeth Adriane Fittschen is an editorial board member of SAB. Her role as editorial board member, had no involvement in the peer review of this article and had no access to information regarding its peer review. Full responsibility for the editorial process for this article was delegated to another journal editor. If there are other authors, they declare that they have no known competing financial interests or personal relationships that could have appeared to influence the work reported in this paper.

Acknowledgments

This article/publication is based upon work from COST Action CA18130 ENFORCE TXRF, supported by COST (European Cooperation in Science and Technology). COST (European Cooperation in Science and Technology) is a funding agency for research and innovation networks. Our Actions help connect research initiatives across Europe and enable scientists to grow their ideas by sharing them with their peers. This boosts their research, careers, and innovations. http://www.cost.eu/.

The authors gratefully thank Cedric Jünemann (Clausthal University of Technology, Institute of Physical Chemistry) for the idea on including the influences of static charge on the sample carriers in this study and also for the help with the atomic force microscope. Also we thank Arne Langhoff (Clausthal University of Technology, Institute of Physical Chemistry) for providing the static eliminator. The authors thank Nicolò Di Novo (Fundazione Bruno Kessler) for the assistance with the contact angle measurements.

Appendix A. Supplementary data

Supplementary material related to this article can be found online at https://doi.org/10.1016/j.sab.2026.107586.

Data availability

Data will be made available on request.

References

[1] I. De La Calle, N. Cabaleiro, V. Romero, I. Lavilla, C. Bendicho, Sample pretreatment strategies for total reflection X-ray fluorescence analysis: A tutorial review, Spectrochim. Acta Part B: At. Spectrosc. 90 (2013) 23–54, http://dx.doi.org/10.1016/j.sab.2013.10.001.

[2] R. Klockenkämper, A. von Bohlen, Total-Reflection X-Ray Fluorescence Analysis and Related Methods, vol. 181, Wiley, 2015.

[3] R.D. Deegan, O. Bakajin, T.F. Dupont, G. Huber, S.R. Nagel, T.A. Witten, Capillary flow as the cause of ring stains from dried liquid drops, Nature 389 (6653) (1997) 827–829, http://dx.doi.org/10.1038/39827.

[4] S. Hampel, F. Sand, H.S. Till, U.E.A. Fittschen, Empirical evaluation of the TXRF detector field of view – a coffee-ring case study, J. Anal. At. Spectrom. 39 (2024) 131–140, http://dx.doi.org/10.1039/D3JA00316G.

[5] S. Hampel, F. Sand, D.A. Murcia Gonzalez, G. Pepponi, G. Helsch, J. Deubener, T. Schirmer, A. Fittschen, U.E.A. Fittschen, Chelate complexed multi-elemental printing performance of a small and cost efficient picoliter droplet printing device for micro preparation, Spectrochim. Acta Part B: At. Spectrosc. 206 (2023) 106716, http://dx.doi.org/10.1016/j.sab.2023.106716.

[6] C.M. Sparks, U.E.A. Fittschen, G.J. Havrilla, Picoliter solution deposition for total reflection X-ray fluorescence analysis of semiconductor samples, Spectrochim. Acta Part B: At. Spectrosc. 65 (9–10) (2010) 805–811, http://dx.doi.org/10.1016/j.sab.2010.07.003.

[7] R. Unterumsberger, B. Beckhoff, A. Gross, H. Stosnach, S. Nowak, Y.P. Stenzel, M. Krämer, A. von Bohlen, A round robin test for total reflection X-ray fluorescence analysis using preselected and well characterized samples, J. Anal. At. Spectrom. 36 (2021) 1933–1945, http://dx.doi.org/10.1039/D1JA00103E.

[8] U.E.A. Fittschen, S. Hauschild, M.A. Amberger, G. Lammel, C. Streli, S. Förster, P. Wobrauschek, C. Jokubonis, G. Pepponi, G. Falkenberg, J.A.C. Broekaert, A new technique for the deposition of standard solutions in total reflection X-ray fluorescence spectrometry (TXRF) using pico-droplets generated by inkjet printers and its applicability for aerosol analysis with SR-TXRF, Spectrochim. Acta Part B: At. Spectrosc. 61 (10–11) (2006) 1098–1104, http://dx.doi.org/10.1016/j.sab.2006.09.009, TXRF-2005, 11th International Conference on Total Reflection X-ray Fluorescence Spectrometry and Related Methods.

[9] U.E.A. Fittschen, G.J. Havrilla, Picoliter droplet deposition using a prototype picoliter pipette: control parameters and application in micro X-ray fluorescence, Anal. Chem. 82 (1) (2010) 297–306, http://dx.doi.org/10.1021/ac901979p.

[10] M. Singh, H.M. Haverinen, P. Dhagat, G.E. Jabbour, Inkjet printing—Process and its applications, Adv. Mater. 22 (6) (2010) 673–685, http://dx.doi.org/10.1002/adma.200901141.

[11] J.G. Korvink, P.J. Smith, D.-Y. Shin, Inkjet-based Micromanufacturing, Wiley-VCH, Weinheim, 2012.

[12] G. Cummins, M.P.Y. Desmulliez, Inkjet printing of conductive materials: a review, Circuit World 38 (4) (2012) 193–213, http://dx.doi.org/10.1108/03056121211280413.

[13] S.D. Hoath, Fundamentals of Inkjet Printing: The Science of Inkjet and Droplets, Wiley-VCH, Weinheim, 2016.

[14] HP Extended TIJ 1.0 Print Cartridges, Hewlett-Packard Development Company, L.P., 2003.

[15] R.T. van Gaalen, C. Diddens, H.M.A. Wijshoff, J.G.M. Kuerten, Marangoni circulation in evaporating droplets in the presence of soluble surfactants, J. Colloid Interface Sci. 584 (2021) 622–633, http://dx.doi.org/10.1016/j.jcis.2020.10.057.

[16] R. Fernández-Ruiz, A brief revision of the suspension-assisted direct solid analysis by TXRF spectrometry, Spectrochim. Acta Part B: At. Spectrosc. 229 (2025) 107214, http://dx.doi.org/10.1016/j.sab.2025.107214.

[17] S. Hauschild, Herstellung Von Kolloidalen Dispersionen Und Oberflächenbeschichtungen Mit Tintendruckern (Ph.D. thesis), University of Hamburg, 2009.

[18] S. Magdassi, The Chemistry of Inkjet Inks, WORLD SCIENTIFIC Publishing Co. Pte. Ltd., Singapore, 2010.

[19] S.H. Behrens, D.G. Grier, The charge of glass and silica surfaces, J. Chem. Phys. 115 (14) (2001) 6716–6721, http://dx.doi.org/10.1063/1.1404988.

[20] Y. Jin, C. Wu, P. Sun, M. Wang, M. Cui, C. Zhang, Z. Wang, Electrification of water: From basics to applications, Droplet 1 (2) (2022) 92–109, http://dx.doi.org/10.1002/dro2.22.

[21] S. Haeberle, R. Zengerle, Microfluidic platforms for lab-on-a-chip applications, Lab Chip 7 (2007) 1094–1110, http://dx.doi.org/10.1039/B706364B.

[22] A. von Bohlen, M. Krämer, C. Sternemann, M. Paulus, The influence of X-ray coherence length on TXRF and XSW and the characterization of nanoparticles observed under grazing incidence of X-rays, J. Anal. At. Spectrom. 24 (2009) 792–800, http://dx.doi.org/10.1039/B811178B.

[23] H.S. Till, A. Gross, U.E.A. Fittschen, Exploring the boundaries of double excitation in TXRF, Spectrochim. Acta Part B: At. Spectrosc. 225 (2025) 107138, http://dx.doi.org/10.1016/j.sab.2025.107138.

[24] H. Schwenke, W. Berneike, J. Knoth, U. Weisbrod, How to use the features of total reflection of X-rays for energy dispersive XRF, Adv. X-Ray Anal. 32 (1988) 105–114, http://dx.doi.org/10.1154/S037603080002036X.

[25] D.K.G. de Boer, W.W. van den Hoogenhof, Total-reflection X-ray fluorescence of thin layers on and in solids, Adv. X-Ray Anal. 34 (1990) 35–40, http://dx.doi.org/10.1154/S0376030800014312.

[26] D.K.G. de Boer, Glancing-incidence x-ray fluorescence of layered materials, Phys. Rev. B 44 (1991) 498–511, http://dx.doi.org/10.1103/PhysRevB.44.498.

[27] V. Szwedowski-Rammert, J. Baumann, C. Schlesiger, U. Waldschläger, A. Gross, B. Kanngießer, I. Mantouvalou, Laboratory based GIXRF and GEXRF spectrometers for multilayer structure investigations, J. Anal. At. Spectrom. 34 (2019) 922–929, http://dx.doi.org/10.1039/C8JA00427G.

[28] C. Morawe, J.-C. Peffen, E.M. Dufresne, Y.S. Chu, A.T. Macrander, Double gradient multilayers for broadband focusing, Proc SPIE 5195 (2003) 1–11, http://dx.doi.org/10.1117/12.502658.

[29] D. Ingerle, G. Pepponi, F. Meirer, P. Wobrauschek, C. Streli, JGIXA — A software package for the calculation and fitting of grazing incidence X-ray fluorescence and X-ray reflectivity data for the characterization of nanometer-layers and ultra-shallow-implants, Spectrochim. Acta Part B: At. Spectrosc. 118 (2016) 20–28, http://dx.doi.org/10.1016/j.sab.2016.02.010.

[30] F. Brigidi, G. Pepponi, GIMPy: a software for the simulation of X-ray fluorescence and reflectivity of layered materials, X-Ray Spectrom. 46 (2) (2017) 116–122, http://dx.doi.org/10.1002/xrs.2746.

[31] A.M. Haveen, D.A. Jameel, Modeling and the main stages of spin coating process: A review, J. Appl. Sci. Technol. Trends 2 (3) (2021) 91–95, http://dx.doi.org/10.38094/jastt203109.

[32] K. Danzer, Analytical Chemistry: Theoretical and Metrological Fundamentals, Springer Berlin Heidelberg, 2007, http://dx.doi.org/10.1007/b103950.

[33] I. Rink, P. Rostam-Khani, J. Knoth, H. Schwenke, S. de Gendt, R. Wortelboer, Calibration of straight total reflection X-ray fluorescence spectrometry — results of a European round robin test, Spectrochim. Acta Part B: At. Spectrosc. 56 (11) (2001) 2283–2292, http://dx.doi.org/10.1016/S0584-8547(01)00297-X, 8TH CONFERENCE ON TOTAL REFLECTION X-RAY FLUORESCENCE ANALYSIS AND RELATED METHODS.

[34] K. Tsuji, N. Taniguchi, H. Yamaguchi, T. Matsuyama, Evaluation of analysis volume in total reflection X-ray fluorescence analysis, X-Ray Spectrom. 52 (6) (2023) 357–363, http://dx.doi.org/10.1002/xrs.3335.

[35] J. Haberl, S. Fromm, M. Schuster, Digestions vs. suspensions: The influence of sample preparation on precision and accuracy in total-reflection X-ray fluorescence analysis by the example of waste incineration fly ash, Spectrochim. Acta Part B: At. Spectrosc. 154 (2019) 82–90, http://dx.doi.org/10.1016/j.sab.2019.02.004.

[36] S. Hampel, Study on 3D- and Picoliter Printed Multi-Elemental References and Element Species Properties with Respect to Energy Storage and Recycling (Ph.D. thesis), Clausthal University of Technology, 2024, http://dx.doi.org/10.21268/20241121-0.

[37] H.S. Till, Evaluation of the Grazing Incidence XRF capacities of a prototype Total Reflection XRF spectrometer to analyze thin films and Nanoparticles (Master thesis), Clausthal University of Technology, 2020, http://dx.doi.org/10.21268/20260512-0.

[38] V.A. Solé, E. Papillon, M. Cotte, P. Walter, J. Susini, A multiplatform code for the analysis of energy-dispersive X-ray fluorescence spectra, Spectrochim. Acta Part B: At. Spectrosc. 62 (1) (2007) 63–68, http://dx.doi.org/10.1016/j.sab.2006.12.002.

[39] F.E. Grubbs, Sample criteria for testing outlying observations, Ann. Math. Stat. 21 (1950) 27–58, http://dx.doi.org/10.1214/aoms/1177729885.

[40] F.E. Grubbs, Procedures for detecting outlying observations in samples, Technometrics 11 (1) (1969) 1–21, http://dx.doi.org/10.1080/00401706.1969.10490657.

[41] C.A. Schneider, W.S. Rasband, K.W. Eliceiri, NIH image to ImageJ: 25 years of image analysis, Nat. Methods 9 (7) (2012) 671–675, http://dx.doi.org/10.1038/nmeth.2089.

[42] A.F. Stalder, G. Kulik, D. Sage, L. Barbieri, P. Hoffmann, A snake-based approach to accurate determination of both contact points and contact angles, Colloids Surfaces A: Physicochem. Eng. Aspects 286 (1) (2006) 92–103, http://dx.doi.org/10.1016/j.colsurfa.2006.03.008.

[43] A.F. Stalder, T. Melchior, M. Müller, D. Sage, T. Blu, M. Unser, Low-bond axisymmetric drop shape analysis for surface tension and contact angle measurements of sessile drops, Colloids Surfaces A: Physicochem. Eng. Aspects 364 (2010) 72–81, http://dx.doi.org/10.1016/j.colsurfa.2010.04.040.

[44] D. Nečas, P. Klapetek, Gwyddion: an open-source software for SPM data analysis, Central Eur. J. Phys. 10 (2012) 181–188, http://dx.doi.org/10.2478/s11534-011-0096-2.

[45] P. Klapetek, D. Nečas, Gwyddion - Free SPM (AFM, SNOM/NSOM, STM, MFM,...) data analysis software, 2018, URL https://gwyddion.net/ last accessed on 2026-03-10.

[46] P. Klapetek, D. Nečas, C. Anderson, Gwyddion user guide, 2026, URL https://gwyddion.net/download/user-guide/gwyddion-user-guide-en.pdf last accessed on 2026-03-10.

[47] K. Tsuji, T. Matsuyama, T. Fukuda, S. Shima, M. Toba, J.-S. Oh, T. Shirafuji, Total reflection X-ray fluorescence analysis with a glass substrate treated with a He atmospheric pressure plasma jet, J. Anal. At. Spectrom. 36 (2021) 1873–1878, http://dx.doi.org/10.1039/D1JA00164G.

[48] G. Schwarzenbach, R. Gut, G. Anderegg, Komplexone XXV. Die polarographische untersuchung von austauschgleichgewichten. Neue daten der bildungskonstanten von metallkomplexen der äthylendiamin-tetraessigsäure und der 1,2-diaminocyclohexan-tetraessigsäure, Helvetica Chimica Acta 37 (4) (1954) 937–957, http://dx.doi.org/10.1002/hlca.19540370402.

[49] K. Hermansson, U. Lindberg, B. Hok, G. Palmskog, Wetting properties of silicon surfaces, in: TRANSDUCERS '91: 1991 International Conference on Solid-State Sensors and Actuators. Digest of Technical Papers, 1991, pp. 193–196, http://dx.doi.org/10.1109/SENSOR.1991.148835.

[50] X.M. Yang, Z.W. Zhong, E.M. Diallo, Z.H. Wang, W.S. Yue, Silicon wafer wettability and aging behaviors: Impact on gold thin-film morphology, Mater. Sci. Semicond. Process. 26 (2014) 25–32, http://dx.doi.org/10.1016/j.mssp.2014.03.044.

[51] J.-G. Park, S. Raghavan, Dynamic wetting behavior of silicon wafers in alkaline solutions of interest to semiconductor processing, J. Adhes. Sci. Technol. 7 (3) (1993) 179–193, http://dx.doi.org/10.1163/156856193X00646.

[52] G. Gould, E.A. Irene, An in situ ellipsometric study of aqueous NH 4 OH treatment of silicon, J. Electrochem. Soc. 136 (4) (1989) 1108–1112, http://dx.doi.org/10.1149/1.2096794.

[53] H.-S. Hwang, J.-H. Park, E.-S. Choi, J.-W. Ahn, J.-G. Park, Effect of NH4OH concentration on surface qualities of a silicon wafer after final-touch polishing, J. Electrochem. Soc. 158 (6) (2011) H641–H644, http://dx.doi.org/10.1149/1.3571006.

[54] B. Wiggershaus, E. Franke, C. Vogt, Total reflection x-ray fluorescence analysis of trace elements in highly saline samples, X-Ray Spectrom. 54 (2) (2025) 193–202, http://dx.doi.org/10.1002/xrs.3448.